



Universidade de São Paulo

Biblioteca Digital da Produção Intelectual - BDPI

Departamento de Física e Ciências Materiais - IFSC/FCM

Artigos e Materiais de Revistas Científicas - IFSC/FCM

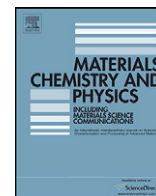
2011

An improved method for preparation of SrTi'O IND.3' nanoparticles

Materials Chemistry and Physics, Lausanne : Elsevier, v. 125, p. 168-173, 2011

<http://www.producao.usp.br/handle/BDPI/49353>

Downloaded from: Biblioteca Digital da Produção Intelectual - BDPI, Universidade de São Paulo



An improved method for preparation of SrTiO₃ nanoparticles

L.F. da Silva^a, L.J.Q. Maia^b, M.I.B. Bernardi^a, J.A. Andrés^c, V.R. Mastelaro^{a,*}

^a Instituto de Física de São Carlos, USP, São Carlos, SP, Brazil

^b Instituto de Física, UFG, Goiânia, GO, Brazil

^c Departamento de Química Física y Analítica, Universitat Jaume I, 12071 Castelló, Spain

ARTICLE INFO

Article history:

Received 13 January 2010

Received in revised form 17 August 2010

Accepted 1 September 2010

Keywords:

Chemical synthesis

Calcination

Nanostructure

Photoluminescence spectroscopy

ABSTRACT

SrTiO₃ nanoparticles were synthesized for the first time via a modified polymeric precursor method. The samples were characterized by thermogravimetry, X-ray diffraction (XRD), BET surface area, micro-Raman spectroscopy, field emission scanning and transmission electron microscopy (FE-SEM and FE-STEM), high-resolution transmission electron microscopy (HRTEM) and photoluminescence measurements. It is found that calcination atmosphere (air, nitrogen and oxygen) plays an important role of both crystal size and photoluminescence behavior of the SrTiO₃ nanocrystallites. Results show that the powders obtained in nitrogen/oxygen atmosphere possess controllable particles size of approximately 11 nm presenting the highest photoluminescence emission.

© 2010 Elsevier B.V. All rights reserved.

1. Introduction

Nanostructured materials have been generating tremendous interests in the past years due to their fundamental significance for addressing some basic issues in fundamental physics, as well as their potential applications as advanced materials with collective properties [1]. Perovskite-type oxides are some of the most fascinating materials in condensed-matter research. Strontium titanate, SrTiO₃ (STO), is arguably the prototypical member of this structure family, not only because it can be made to exhibit a diverse range of unusual properties itself. Moreover, STO is an important *n*-type semiconductor with band gap of about 3.2 eV [2], and it has been widely studied not only because of its variety of outstanding physical properties (stability, wavelength response, and current–voltage) but also for its practical applications, such as their high static dielectric constant and good insulation [3,4], their use in grain boundary barrier-layer capacitors [5], resistive oxygen gas sensors [6,7], solar cells [8], solid oxide electronic device [9], at large scale, as substrate at the time of growth of thin films perovskite compounds [10], and promising candidate for efficient photocatalysts [11] and photoelectrodes [12,13].

It is well known that the properties of nanoparticles depend not only of the synthesis method and chemical composition but also on their structure, shape, and size. Therefore, the ability to tune the size and shape of STO particles is significant for fundamental studies as well as for the preparation of ceramics and composite materi-

als with tailored properties. There were many synthesis methods applied to prepare pure and doped STO, including solid-state reaction [14], sol–gel method [15,16], micro-emulsion method [17], hydrothermal synthesis [18–21], and the polymeric precursor method [22–24]. Recently, controlled homogeneity of the precursor gel in the synthesis of STO nanoparticles by an epoxide-assisted sol–gel route was reported by Cui et al. [25]. However, it is found that the obtained STO nanoscale particles are agglomeration or have irregular morphology.

Alternatively, microwave assisted hydrothermal method has been newly developed for the preparation of perovskite based materials [26–28]. Among these synthetic procedures, the polymeric precursor method, also called the Pechini route, offers interesting advantages such as good control of stoichiometry, easy reproducibility and mainly, the possibility of obtaining nanometric particles size [22–24]. It is well established that morphology and grain size are directly related with the dielectric properties and polarization of ferroelectric and related materials [29]. Recently, different researchers obtained nanosized oxide compounds with different particle sizes and shapes as a result of different calcination routes [30,31]. They observed that when they heat-treated their samples in a nitrogen atmosphere at a high temperature prior to heat-treating at a lower temperature in air or oxygen atmospheres, they could prevent the crystal growth process of the nanoparticles, thereby achieving a smaller and narrower particle size distribution. Xie et al. explained this behavior by the fact that, when the samples were heat-treated under the nitrogen atmosphere, the organic citrate in the sample was not burned up but decomposed into ultrafine carbon powders, which can encapsulate or isolate the nanoparticles and prevent their growth during the sintering process [30]. Subsequent calcination in air at a low temperature removed the carbon

* Corresponding author. Tel.: +55 16 3373 9828; fax: +55 16 3373 9824.
E-mail address: valmor@ifsc.usp.br (V.R. Mastelaro).

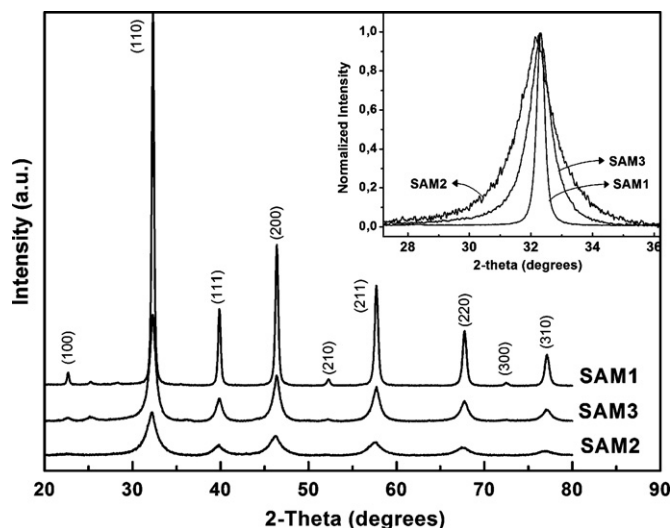


Fig. 1. XRD patterns of SrTiO₃ nanoparticles after calcination. The inset shows the normalized intensity of the (1 1 0) diffraction peak.

species completely, resulting in a sample with nanoparticles of less than 10 nm and a high specific surface area.

Motivated by these considerations, in this paper we report the synthesis and characterization of STO nanoparticles, with a remarkable small size and high surface area, obtained by modified polymeric precursor method. Sample characterizations are carried out using a variety of experimental techniques. These include X-ray diffraction (XRD), surface area measurements, micro-Raman spectroscopy, room temperature photoluminescence (PL) measurements, field emission scanning electron microscopy (FE-SEM) and scanning transmission electron microscope (FE-STEM) and transmission electron microscope (HRTEM) techniques. Our aim is to study the effect of the annealing conditions (temperature and kind of atmosphere) on the nanoparticles' size, structural and microstructural, as well as on the luminescence characteristics. Finally, a mechanism to explain the formation of nanoparticles with a smaller particle size distribution is proposed. The paper is organized as follows: Section 2 describes the experimental techniques and equipments. The results and discussion are presented in Section 3. The final section of conclusions is a summary of our main results.

2. Experimental techniques and equipments

The STO powders studied in the present work were synthesized following a soft chemical method, the so-called polymeric precursors method and details of the processing have already been published elsewhere [32]. The polymeric precursor solution was heat-treated at 300 °C for 8 h at a heating rate of 10 °C min⁻¹. Then, the obtained powder was grounded in an agate mortar in order to deagglomerate the powder, called the "precursor". Part of the precursor powder was heat-treated at 750 °C for 2 h in an electric furnace under air atmosphere, applying a heating rate of 10 °C min⁻¹; this sample was denoted as sample SAM1. The remaining precursor powder was heat-treated at 750 °C under a nitrogen atmosphere and was denoted as sample SAM2. The latter sample was then calcined at 400 °C for 4 h under a rich oxygen atmosphere (denoted as sample SAM3).

The samples were characterized structurally by X-ray diffraction (XRD) in a 2θ range from 20 to 80° with a step of 0.020°, at a scanning speed of 2° min⁻¹, at room temperature using Cu Kα radiation (Rigaku, Rotaflex RU200B). Raman spec-

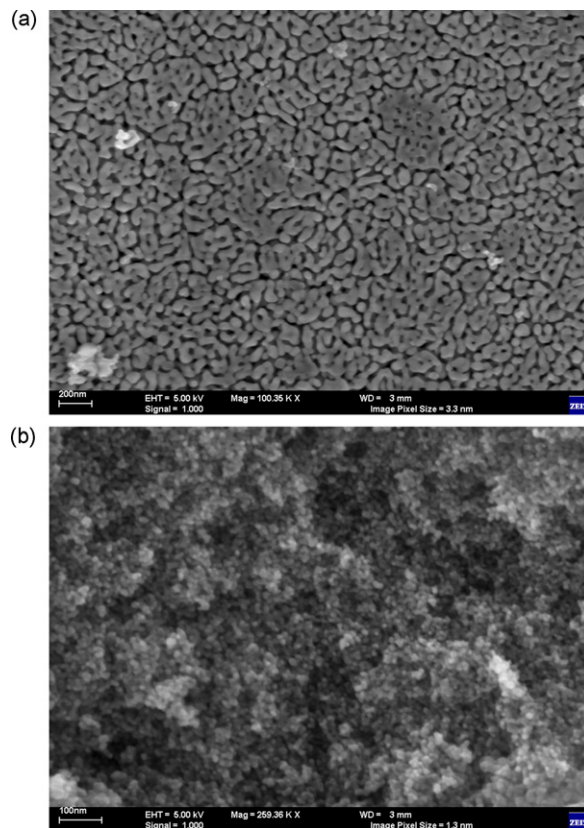


Fig. 2. FE-SEM images of SrTiO₃ nanoparticles: (a) SAM1 sample and (b) SAM3 sample.

tra were registered at room temperature with a micro-Raman Renishaw R2000 system. The samples were excited with a 632.8 nm He-Ne line. The Raman spectra were collected between 1000 cm⁻¹ and 2000 cm⁻¹ and the spectral resolution stays around 1 cm⁻¹. The surface area of the SrTiO₃ nanoparticles was obtained using a Brunauer–Emmett–Teller (BET) method (ASAP2000, Micrometrics Instrument Corp.). Particle size (d_{BET}) was calculated using the equation $d_{\text{BET}} = (6/S_{\text{BET}}\rho)$, where S_{BET} is the BET surface area and ρ is the theoretical density of the studied phases. Photoluminescence spectra were collected at room temperature with a Thermal Jarrel-Ash Monospec 27 monochromator and a Hamamatsu R446 photomultiplier. The 350 nm exciting wavelength of a krypton ion laser (Coherent Innova) was used, with the nominal output power kept at 550 mW. The morphology of STO nanoparticles was investigated by field emission scanning electron microscopy (FE-SEM) and scanning transmission electron microscope (FE-STEM) (Supra 35-VP, Carl Zeiss) operating at 5 kV in SEM mode and 23 kV in TEM mode. The mean particle size was estimated from the analysis of SEM micrographs through the measure of approximately 100 nanoparticles. The size and morphology of the as-obtained samples were also determined using a JEOL JEM 2010 URP high-resolution transmission electron microscopy (HRTEM) operating at 200 KeV.

3. Results and discussion

The XRD pattern of the as-prepared STO samples is shown in Fig. 1. All the diffraction peaks can be indexed to a cubic perovskite structure of STO with lattice constant $a = 3.90 \text{ \AA}$, which is in good agreement with the literature value (JCPDS: 35-0734). The strong and sharp peaks suggest that STO crystals are highly crystalline. Two peaks of SrCO₃ phase (JCPDS: 05-0418) were also

Table 1

Average crystallite size obtained from XRD patterns, BET surface area, BET particle size (d_{BET}) and average particle size obtained from FE-SEM image.

Sample	Average XRD crystallite size (nm)	BET surface area (m ² g ⁻¹)	d_{BET} Particle size (nm)	FE-SEM average particle size (nm)
SAM1	39	16	73	65 ± 3
SAM2	7	*	*	*
SAM3	11	83	14	10.8 ± 0.4

* Not measured.

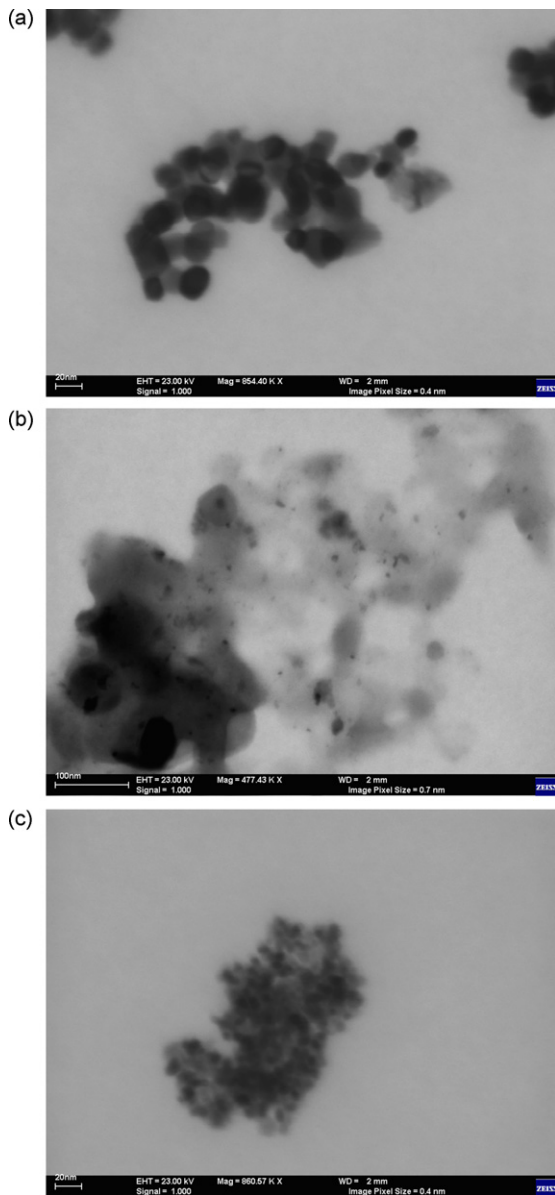


Fig. 3. FE-STEM images of SrTiO₃ nanoparticles: (a) SAM1 sample, (b) SAM2 sample and (c) SAM3 sample.

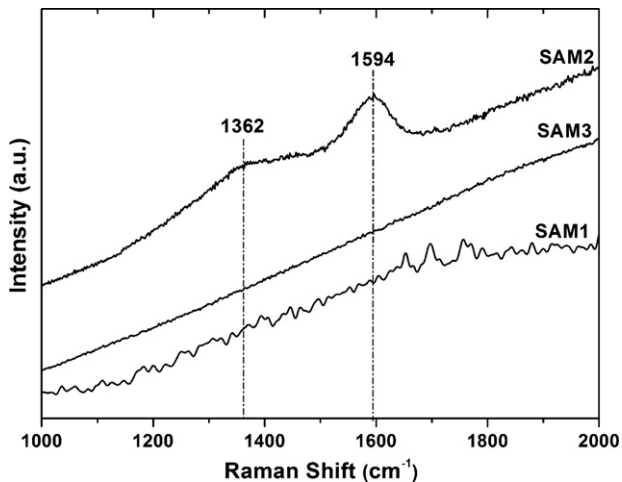


Fig. 4. Micro-Raman spectra of samples SAM1, SAM2, and SAM3. The presence of carbon is detected by the presence of broad peaks at 1362 and 1594 cm⁻¹.

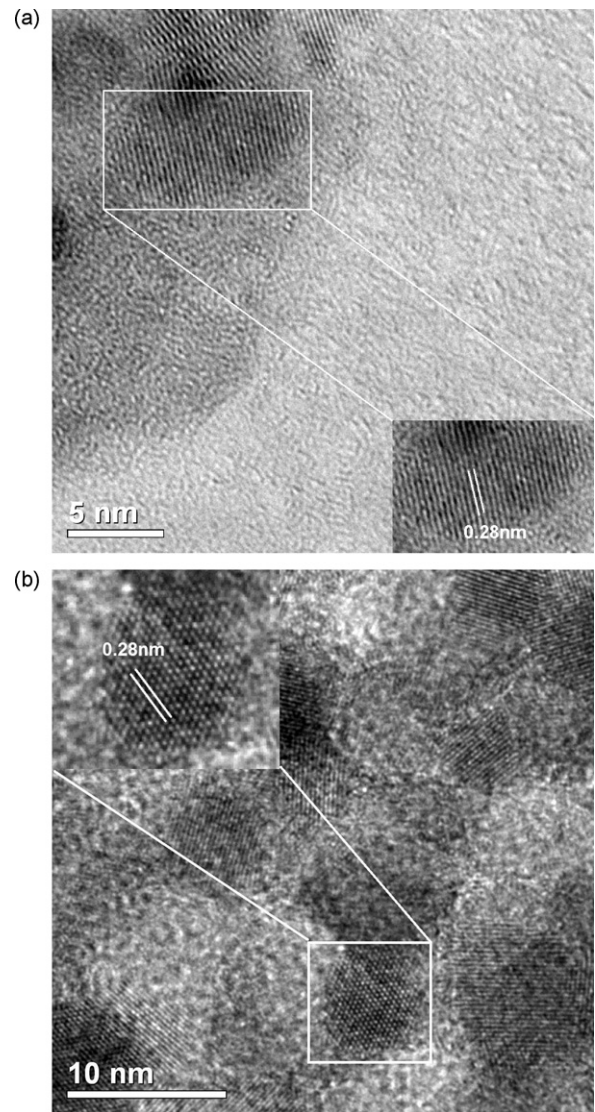


Fig. 5. HRTEM images of: (a) SAM2 and (b) SAM3 samples. The inset in Fig. 5a and b shows the distance between (1 1 0) STO crystallographic planes.

observed at 25.2° and 36°, except in the SAM2 sample. The diffraction patterns of SAM2 and SAM3 samples displayed broader peaks with lower intensities than the SAM1 sample indicating that the heat-treatment under the nitrogen atmosphere produced smaller crystallite sizes. On the other hand, among the powders calcined under nitrogen, we found that sample SAM3 present a higher degree of crystallinity characterized by a higher peak intensity associated with a lower full-width-at-half-maximum (FWHM) than the SAM2 sample (inset of Fig. 1). Thus, XRD results revealed the strong influence of the calcination environment on the degree of crystallization. The subsequent heat treatment at 400 °C under oxygen led to the removal of the remaining carbon, which, according to the literature and thermogravimetric (TG) measurements (not showed), is released as carbon monoxide and dioxide [33].

The average crystallite size of nanoparticles was calculated from the FWHM of (1 1 0) diffraction reflection using Scherrer's equation [34]. The FWHM value of the diffraction peak due to instrumental broadening was considered using silicon powder as a standard sample. The BET mean particle size (d_{BET}) was estimated from specific surface area (S_{BET}) measured using BET method [35]. Table 1 shows the average XRD crystallite size, BET specific surface area (S_{BET}) and BET particle size (d_{BET}) and the average particle size estimated from

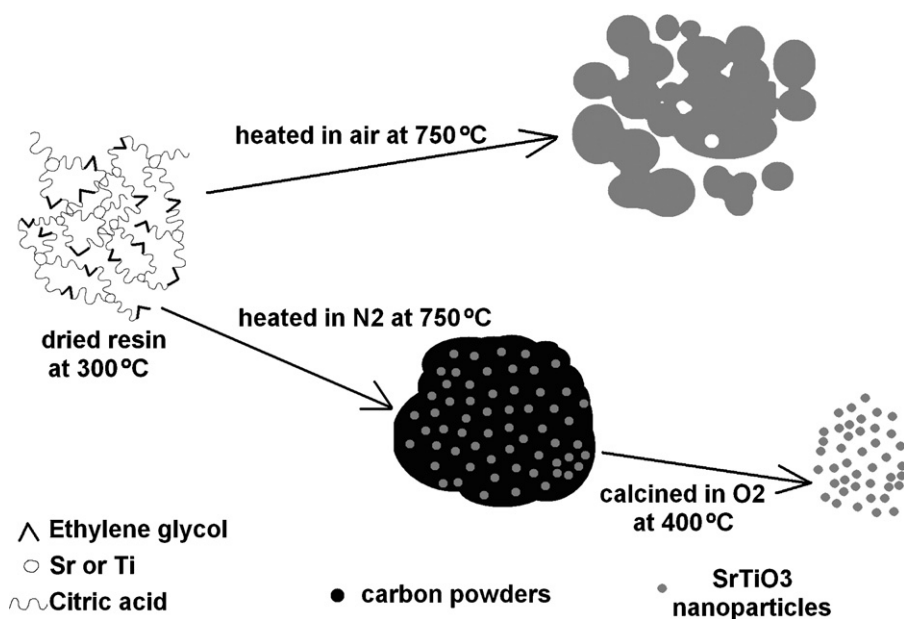


Fig. 6. Schematic diagram of the mechanism of the formation of SrTiO₃ nanoparticles according to the atmosphere and the temperature used during the synthesis (Chen et al., [30]; Xie et al. [31]).

FE-SEM images of the samples calcined under different environments. Note that, in comparison with SAM1 sample, the sample calcined at 750 °C in the nitrogen atmosphere and subsequently at 400 °C in oxygen atmosphere (SAM3 sample) presents a crystallite and a particle size significantly smaller and a higher specific surface area. As it is well known, many chemical and physical processes and properties, such as crystal growth, crystal morphology, and adsorption are controlled by the surface energy. Therefore, these results point out that the particle growth and the reduction of surface area are inhibited by the heat treatment under nitrogen atmosphere.

The FE-SEM micrographs of samples after thermal treatments in different atmospheres are presented in Fig. 2. The micrograph of SAM1 sample calcined in air (Fig. 2a) shows strongly agglomerated nonuniform particles with neck formation and coalescence between the nanoparticles. On the other hand, as can be observed in Fig. 2b, the sample heat-treated under nitrogen and subsequently in oxygen atmospheres, i.e., sample SAM3, exhibits quasi-spherical particles and a sharp nanoparticle size distribution. Although SAM3 sample showed a certain degree of agglomeration, no neck formation or coalescence phenomena were observed in this sample. Moreover, as can be observed in Table 1, the analysis of FE-SEM images confirm a significant reduction of SAM3 sample average particle size in comparison to that of SAM1 sample.

In order to support the presence of amorphous carbon around STO nanoparticles and the reduction on the particle size, FE-STEM and HRTEM images as well as micro-Raman measurements were carried in the samples. Fig. 3 shows scanning transmission electron microscopy FE-STEM images of STO nanoparticles heat-treated at different atmospheres and temperatures. Like the FE-SEM images (Fig. 2a), the FE-STEM image of the sample calcined only in air (SAM1), shows a large particle size distribution and the formation of necks and coalescence. The FE-STEM image of the sample calcined only under the nitrogen atmosphere (SAM2, Fig. 3b) clearly shows the formation of carbon agglomerates containing embedded smaller SrTiO₃ nanoparticles.

Fig. 4 shows the micro-Raman spectra of samples. As expected, the micro-Raman spectrum of SAM1 sample does not display any peak, due the first-order Raman scattering is forbidden in a cubic structure [36]. On the other hand, the micro-Raman spectrum of SAM2 sample shows the presence of two broad peaks, D and

G, at around 1360 and 1590 cm⁻¹ that, according to the literature, are characteristics of amorphous carbon [37,38]. The FE-STEM image and micro-Raman spectrum of SAM3 sample (Figs. 3c and 4 respectively), shows that the heat-treatment at low-temperature under oxygen of the nanoparticles previously calcined under nitrogen atmosphere removed the amorphous carbon and revealed the formation of smaller STO nanoparticles, which is consistent with FE-SEM results.

The structure, morphology and particle size of SAM2 and SAM3 samples were also investigated by high-resolution transmission electron microscopy (HRTEM). As observed in the XRD pattern of SAM2 sample, on the HRTEM image of SAM2 sample presented in Fig. 5a, it is possible to observe that the distance between neighboring planes is around 0.28 nm (inset in Fig. 5a), which is consistent with the (1 1 0) plane in the cubic perovskite structure of STO. In good agreement with FE-SEM and BET results, HRTEM image of SAM3 presented in Fig. 5b shows the presence of quasi-spherical nanoparticles with size around 10 nm. Moreover, as is shown in the inset of Fig. 5b, the heat-treatment at low-temperature under oxygen of the nanoparticles previously calcined under nitrogen atmosphere does not affect the STO structure.

According to the literature, the formation of agglomerates and nonuniform particles probably occurs due the excess heat released by the burnout of organic residues, which promotes partial sintering of the particles [22,35]. Our FE-SEM and FE-STEM results clearly indicate that when the same powder precursor was burned under the nitrogen atmosphere, the organic material was not completely decomposed, forming carbon agglomerates containing dispersed STO nanoparticles.

Based on previous works [30,31] and on the results presented in this paper, we propose in Fig. 6 a schematic diagram for the formation of STO nanoparticles as a function of the calcination atmosphere and temperature. The nanoparticles growth was precluded by the presence of carbon surrounding the particles, which did not allow the grain boundary to move toward the smaller particles, preventing their growth and coalescence.

Fig. 7 shows the photoluminescence (PL) spectra recorded at room temperature for the samples heat-treated in air (SAM1) in nitrogen atmosphere (SAM2) and in nitrogen atmosphere followed by a treatment in oxygen atmosphere (SAM3). We can observe that

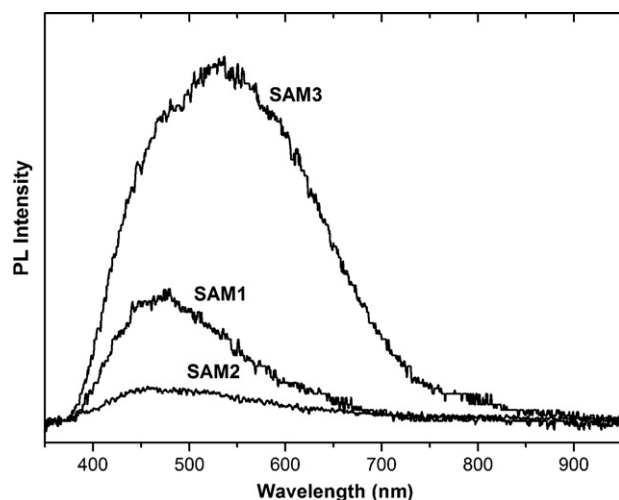


Fig. 7. Room temperature PL spectra of SAM1, SAM2 and SAM3 samples.

the intensity of PL emission is higher in the SAM3 sample and lower for the SAM1 and SAM2 samples.

According to the literature, the profile of the PL emission band observed in Fig. 7 can be characterized as typical of a multiphonon process, i.e., a system in which relaxation occurs by several paths, involving the participation of numerous states within the band gap of the material, originating from by intrinsic defects of the material [39–42].

From the structural and morphological point of view, XRD, BET, FE-STEM and HRTEM results shows that all samples are crystalline and the main differences between the samples heat-treated only in air and in nitrogen (and nitrogen and oxygen) are the crystallite and particle sizes and the surface area. It is expected that the samples presenting a smaller particle size and a large surface area will then presents a higher PL emission. This behavior is observed for the SAM3. However, although the SAM2 sample presents a comparable particle size, its PL emission is the lowest. The low PL emission observed on the SAM2 sample could be related to the fact the carbon embedded the STO nanoparticles. The relative lower intensity of PL curve of SAM1 sample was attributed to higher particle size and to the high degree of structural long-range order.

4. Conclusions

We have successfully synthesized the SrTiO₃ (STO) nanoparticles by means of a modified polymeric precursor method at different calcination atmospheres. The prepared STO nanoparticles were thoroughly studied by various characterization techniques aimed at understanding the samples' spectroscopic properties.

FE-STEM microscopy and micro-Raman measurements indicated that most of the carbon not eliminated during calcination at 750 °C under nitrogen can be effectively eliminated by a subsequent calcination at 400 °C under oxygen.

During the crystallization process, this carbon surrounds the particle and prevents the grain boundary from moving toward the smaller particles, limiting the coalescence of particles. A BET and HRTEM measurements clearly shows that this route enabled us to increase the specific surface area of samples in up to five times and to obtain particles with an average size of about 11 nm. Under these conditions, a higher photoluminescence behavior is observed for the sample and a plausible mechanism for this emission is proposed.

This simple and versatile strategy may provide a general way to obtain nanoparticles with the high surface area a smaller size reactivity as a precursor to fabricate ternary complex oxides, such

as MTiO₃ (M = Ca, Sr, Ba). Then, the synthetic process here can be extended to other perovskite oxides.

Acknowledgment

We are grateful to Prof. Edson Roberto Leite by allowing us to use the FE-SEM and FE-STEM facilities and Mr. Rorivaldo Camargo which operated the equipment. We are also grateful to Prof. Antônio Ricardo Zanatta by micro-Raman measurements and Elaine C. Paris by photoluminescence measurements. The authors also would like to thank the Electron Microscopy Laboratory (LME) of Brazilian Síncrotron Light Laboratory (LNLS) for the HRTEM analysis and Waldir Avansi which operated the equipment. We acknowledge the financial support of the Brazilian research funding institution CNPq and FAPESP. J.A. acknowledges Generalitat Valenciana for *Prometeo/2009/053* project, and Spanish Ministry *Ministerio de Ciencia e Innovación* for project CTQ2009-14541-C02.

References

- [1] X.G. Peng, L. Manna, W.D. Yang, J. Wickham, E. Scher, A. Kadavanich, A.P. Alivisatos, *Nature* 404 (2000) 59.
- [2] M. Cardona, *Phys. Rev.* 140 (1965) 651.
- [3] C.L. Jia, K. Urban, S. Hoffmann, R.J. Waser, *Mater. Res.* 13 (1998) 2206.
- [4] J.H. Haeni, P. Irvin, W. Chang, R. Uecker, P. Reiche, Y.L. Li, S. Choudhury, W. Tian, M.E. Hawley, B. Craigo, A.K. Tagantsev, X.Q. Pan, S.K. Streiffer, L.Q. Chen, S.W. Kirchoefer, J. Levy, D.G. Schlom, *Nature* 430 (2004) 758.
- [5] P. Balaya, M. Ahrens, L. Kienle, J. Maier, B. Rahmati, S.B. Lee, W. Sigle, A. Pashkin, C. Kuntscher, M. Dressel, *J. Am. Ceram. Soc.* 89 (2006) 2804.
- [6] Y. Hu, O.K. Tan, J.S. Pan, H. Huang, W. Cao, *Sens. Actuators B* 108 (2005) 244.
- [7] T. Hara, T. Ishiguro, *Sens. Actuators B* 136 (2009) 489.
- [8] S. Burnside, J.E. Moser, K. Brooks, M. Gratzel, D.J. Cahen, *Phys. Chem. B* 103 (1999) 9328.
- [9] L. Pellegrino, I. Pallecchi, D. Marre, E. Bellingeri, S. Siri, *Appl. Phys. Lett.* 81 (2002) 384.
- [10] M.L. Moreira, J. Andrés, V.M. Longo, M.S. Li, J.A. Varela, E. Longo, *Chem. Phys. Lett.* 473 (2009) 298.
- [11] K. Domen, A. Kudo, T. Onishi, N. Kosugi, H. Kuroda, *J. Phys. Chem.* 90 (1986) 292.
- [12] M.S. Wrighton, A.B. Ellis, P.T. Wolczanski, D.L. Morse, H.B. Abrahamson, D.S. Ginley, *J. Am. Chem. Soc.* 98 (1976) 2774.
- [13] S. Burnside, J.E. Moser, K. Brooks, M.J. Gratzel, *Phys. Chem. B* 103 (1999) 9328.
- [14] H. Tagawa, K. Igarashi, *J. Am. Ceram. Soc.* 69 (1986) 310.
- [15] V.A. Trepakov, M.E. Savinov, I. Okhay, A. Tkach, P.M. Vilarinho, A.L. Kholkin, I. Gregora, L. Jastrabik, *J. Eur. Ceram. Soc.* 27 (2007) 3705.
- [16] G. Pfaff, *J. Mater. Chem.* 7 (1993) 721.
- [17] Q. Pang, J.X. Shi, M.L. Gong, *J. Am. Ceram. Soc.* 90 (2007) 3943.
- [18] P.K. Dutta, J.R. Gregg, *Chem. Mater.* 4 (1992) 843.
- [19] M.-H. Um, H. Kumazawa, *J. Mater. Sci.* 35 (2000) 1295.
- [20] S.C. Zhang, J.X. Liu, Y.X. Han, B.C. Chen, X.G. Li, *Mater. Sci. Eng. B* 110 (2004) 11.
- [21] E.K. Nyutu, C.H. Chen, P.K. Dutta, S.L. Sui, *J. Phys. Chem. C* 112 (2008) 9659.
- [22] E.R. Leite, C.M.G. Sousa, E. Longo, J.A. Varela, *Ceram. Int.* 21 (1995) 153.
- [23] S.M. Zanetti, E. Longo, J.A. Varela, E.R. Leite, *Mater. Lett.* 31 (1997) 173.
- [24] C.H. Chang, Y.H. Shen, *Mater. Lett.* 60 (2006) 129.
- [25] H. Cui, M. Zayat, D. Levy, *J. Non-Cryst. Solids* 353 (2007) 1011.
- [26] M.L. Moreira, J. Andrés, J.A. Varela, E. Longo, *Cryst. Growth Des.* 9 (2009) 833.
- [27] M.L. Moreira, E.C. Paris, G.S. do Nascimento, V.M. Longo, J.R. Sambrano, V.R. Mastelaro, M.I.B. Bernardi, J. Andres, J.A. Varela, E. Longo, *Acta Mater.* 57 (2009) 5174.
- [28] M.L. Moreira, G.P. Mambri, D.P. Volanti, E.R. Leite, M.O. Orlandi, P.S. Pizani, V.R. Mastelaro, C.O. Paiva-Santos, E. Longo, J.A. Varela, *Chem. Mater.* 20 (2008) 5381.
- [29] S. Berger, Y. Drezner, *Ferroelectrics* 327 (2005) 85.
- [30] L.M. Chen, X.M. Sun, Y.N. Liu, Y.D. Li, *Appl. Catal. A: Gen.* 265 (2004) 123.
- [31] G.Q. Xie, M.F. Luo, M. Hei, P. Fang, J.M. Ma, Y.F. Ying, Z.L. Yan, *J. Nanopart. Res.* 9 (2007) 471.
- [32] L.F. da Silva, M.I.B. Bernardi, L.J.Q. Maia, G.J.M. Frigo, V.R. Mastelaro, *J. Therm. Anal. Calorim.* 97 (2009) 173.
- [33] M.K. Cinibulk, *J. Am. Ceram. Soc.* 83 (2000) 1276.
- [34] B.D. Cullity, *Elements of X-ray Diffraction*, 2nd ed., Addison-Wesley Pub. Co., MA, 1978.
- [35] E.R. Leite, M.A.L. Nobre, M. Cerqueira, E. Longo, *J. Am. Ceram. Soc.* 80 (1997) 2649.
- [36] T. Moon, B. Lee, T.G. Kim, J. Oh, Y.W. Noh, S. Nam, S. Park, *Appl. Phys. Lett.* 86 (2005) 182904.
- [37] G. Katumba, B.W. Mwakikunga, T.R. Mothibinyane, *Nanoscale Res. Lett.* 3 (2008) 421.
- [38] A.C. Ferrari, J. Robertson, *Phys. Rev. B* 64 (2001) 075414.

- [39] V.M. Longo, A.T. de Figueiredo, S. De Lazaro, M.F. Gurgel, M.G.S. Costa, C.O. Paiva-Santos, J.A. Varela, E. Longo, V.R. Mastelaro, F.S. De Vicente, A.C. Hernandez, R.W.A. Franco, *J. Appl. Phys.* 104 (2008) 1.
- [40] P.S. Pizani, E.R. Leite, F.M. Pontes, E.C. Paris, J.H. Rangel, E.J.H. Lee, E. Longo, P. Delega, J.A. Varela, *Appl. Phys. Lett.* 77 (2000) 824.
- [41] E. Orhan, F.M. Pontes, C.D. Pinheiro, T.M. Boschi, E.R. Leite, P.S. Pizani, A. Beltrán, J. Andrés, J.A. Varela, E. Longo, *J. Solid State Chem.* 177 (2004) 3879.
- [42] C.D. Pinheiro, E. Longo, E.R. Leite, F.M. Pontes, R. Magnani, J.A. Varela, P.S. Pizani, T.M. Boschi, F. Lanciotti, *Appl. Phys. A* 77 (2003) 81.